On the Inverse Kinematics of Redundant Manipulators: Characterization of the Self-Motion Manifolds

Joel W. Burdick
Dept. of Mechanical Engineering
California Institute of Technology

Abstract

Many previous investigations of redundant manipulator inverse kinematics have been based on instantaneous kinematic methods. This paper takes a global, rather than instantaneous, look at the inverse kinematics of redundant manipulators. This approach is based on a manifold mapping reformulation of manipulator kinematics. While the inverse kinematic problem has an infinite number of solutions for redundant manipulators, the infinity of solutions can be grouped into a finite and bounded set of disjoint continuous manifolds. Each of these manifolds, termed self-motion manifolds, physically corresponds to a distinct self-motion of the manipulator, and the number, geometry, and characterizations of the self-motion manifolds are investigated.

1. Introduction

A manipulator forward kinematic function, f, is a nonlinear vector function which relates a set of n joint coordinates, $\mathbf{q}$, to a set of m end-effector coordinates:

$$\mathbf{x} = f(\mathbf{q}). \tag{1}$$

One of the primary problems of practical interest in manipulator kinematics is determining the inverse kinematic function, f^{-1}, which computes one or more sets of joint angles that place the manipulator end-effector in a desired position and orientation:

$$\mathbf{q} = f^{-1}(\mathbf{x}). \tag{2}$$

For non-redundant manipulators, there is a finite and bounded set of configurations, or "poses," which satisfy (2). For redundant manipulators, there are an infinite number of configurations which satisfy the inverse kinematic relation in (2), although this paper will show that these infinity of solutions can be grouped into a finite set of smooth manifolds.

The redundant degrees of freedom can be used to optimize manipulator properties or perform additional tasks. Consequently, much previous work in redundant manipulator inverse kinematic analysis has been intimately tied to the "redundancy resolution" problem, in which algorithms are developed to determine, or "resolve," the motion of the joints in order to achieve end-effector trajectory control while meeting additional objectives. Many of these previous investigations have focused on the linearized first order instantaneous kinematic relation between end-effector velocities and joint velocities:

$$\dot{\mathbf{x}} = \mathbf{J}(\mathbf{q})\dot{\mathbf{q}} \tag{3}$$

where $\mathbf{J}(\mathbf{q}) = df(\mathbf{q})/d\mathbf{q}$ is the $m \times n$ manipulator Jacobian matrix. When $n > m$, pseudo-inverse techniques [1] can be used to select a solution to (3) from the infinity of possible solutions. A general solution to (3) is:

$$\dot{\mathbf{q}} = \mathbf{J}_W^{\dagger}(\mathbf{q})\,\dot{\mathbf{x}} + (\mathbf{I} - \mathbf{J}_W^{\dagger}(\mathbf{q})\,\mathbf{J}(\mathbf{q}))\mathbf{y}. \tag{4}$$

$\mathbf{J}_W^{\dagger}(\mathbf{q}) = W\mathbf{J}^T(\mathbf{q})(\mathbf{J}(\mathbf{q})W\mathbf{J}^T(\mathbf{q}))^{-1}$ is a weighted pseudo-inverse of the manipulator Jacobian matrix which instantaneously minimizes the symmetric weighted quadratic form $\dot{\mathbf{q}}^T W^{-1}\dot{\mathbf{q}}$ at configuration $\mathbf{q}$. The term $(\mathbf{I} - \mathbf{J}_W^{\dagger}(\mathbf{q})\,\mathbf{J}(\mathbf{q}))$ projects an arbitrary $n \times 1$ vector, $\mathbf{y}$, onto the null space of the manipulator Jacobian matrix. Physically, any motion in the null space is an *instantaneous* motion of the manipulator joints which causes no motion of the end-effector. Many redundancy resolution objectives can be developed as potential functions, and $\mathbf{y}$ might be the gradient of the objective function. In the redundant manipulator literature, the inverse solution to (3) is often referred to as the inverse kinematic solution, rather than (2).

This paper will investigate and characterize the global set of inverse solutions to (2), rather than the linearized version of (3). Some interpretations of the instantaneous solutions in (4) will be considered, but because of space limitations, practical applications of these ideas to redundancy resolution and path planning have been largely omitted. The global analysis of redundant manipulator kinematics is based on a manifold mapping reformulation which considers the aggregate action of the kinematic and inverse kinematic maps on the configuration space manifold. This approach was introduced in [2], and this papers summarizes and corrects some of this work. This approach allows simple topological tools to be applied to the study of manipulator kinematics. Topological methods have been previously used to study manipulator kinematics [3,4,5]. For the particular problems addressed in this paper, few results from topology are needed.

2. A Manifold Mapping Reformulation of Manipulator Kinematics

Only revolute jointed manipulators will be considered in this paper, although other manipulators can be similarly treated. To globally analyze manipulator kinematics, it is useful to rephrase the forward and inverse kinematic problems in terms of manifold mappings. From a point-wise mapping perspective, f maps a joint configuration, $\overline{\theta}$, to an end-effector location: $\mathbf{x} = f(\overline{\theta})$. The set of all possible joint configurations forms a space, termed the "joint space" or "configuration space," which has a simple manifold structure. Similarly, the set of all possible end-effector locations

CH2750-8/89/0000/0264$01.00 © 1989 IEEE

forms the workspace, which also has a manifold structure.

The manifold structure of the joint space arises as follows. Let θ_j denote the joint rotation angle for the j^{th} revolute joint. If the motion of the j^{th} joint is not limited due to mechanical stops, θ_j can take on all values in the interval $[-\pi, \pi]$. However, π and $-\pi$, are equivalent, and their identification yields a circle, denoted by S^1 in Figure 1. The

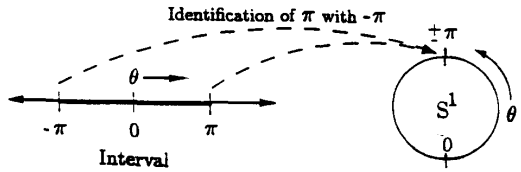

Figure 1: Configuration Space of a Revolute Joint

configuration space, $\mathcal{C}$, of an n-revolute-jointed manipulator is a product space formed by the n-times product of the individual joint manifolds:

$$\mathcal{C} = S^1 \times S^1 \times \cdots \times S^1 = T^n \tag{5}$$

where T^n is an *n-torus*, which is a compact n-dimensional manifold. Each of the circles that make up the torus is termed a *generator* of the torus, and is physically equivalent to a 2π rotation of one joint. There is a one-to-one correspondence between each point in the n-torus configuration space manifold and a distinct manipulator configuration. For example, the $2R$ planar manipulator in Figure 2(a) has a 2-torus configuration space (Figure 2(b)). While the

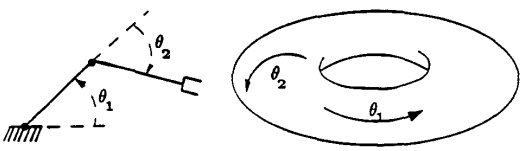

(a) Planar 2R Manipulator **(b) 2-torus Configuration Space Manifold**

Figure 2: Configuration Space of a $2R$ Manipulator

torus geometry properly captures the manifold structure of $\mathcal{C}$, there are times when other representations of the torus are useful. For example, $\mathcal{C}$ in Figure 2 can be presented as a square with dimension 2π by "cutting" the torus along two generators (Figure 3). The 3-torus configuration space of a 3R manipulator can not be directly viewed in a 3-dimensional space, but it can be presented as a cube of dimensions 2π by cutting along the 3-tori generators, and the cubes in the following figures are 3-tori sliced along their generators.

Attach a frame to the manipulator end-effector. The manipulator's workspace manifold, $\mathcal{W}$, is the set of all possible locations and orientations of this frame as the manipulator joints are swept through all points of $\mathcal{C}$. The geometric characterization of $\mathcal{W}$ is more complex than the torus characterization of $\mathcal{C}$, and is considered in [2,6].

Rather than viewing f as a point-wise mapping, one can alternatively view the action of f as *the global rearrangement of the configuration space manifold to produce the workspace manifold*:

$$f(\overline{\theta})\colon \mathcal{C} \rightarrow \mathcal{W}. \tag{6}$$

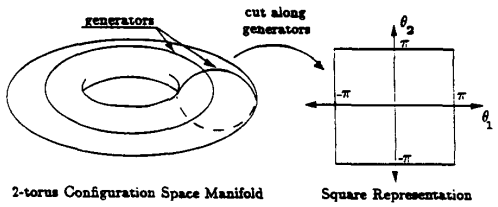

Figure 3: Square Representation of 2-Torus

Roughly speaking, the forward kinematic map "rips" the configuration space manifold apart into pieces; distorts each piece; and combines the distorted pieces to form $\mathcal{W}$. The dividing action of the forward kinematic map is governed by the loci of singularities [2]. The principal problems to be investigated in this paper can be restated as the characterization of the solutions to (2), within the framework established by (6). The global configuration space to workspace mapping in (6) is briefly reviewed in Section 7, and in more detail in [2,6].

3. Redundant Inverse Kinematic Solution: Self-Motion Manifolds

Let $r = (n - m)$ be the relative degrees of redundancy. For non-redundant manipulators, the inverse kinematic solution (also termed a *preimage*) $f^{-1}(\mathbf{x})$ of a regular [1] end-effector location is a bounded set of discrete configurations. It has been shown [7] that a $6R$ manipulator with arbitrary geometry can have up to 16 inverse kinematic solutions.

Since f is a smooth function which maps $\mathcal{C}$, a compact manifold, to $\mathcal{W}$, a redundant manipulator inverse kinematic solution for a regular $\mathbf{x}$ must be an r-dimensional submanifold of $\mathcal{C}$ [8]. However, the preimage submanifold may be divided into more than one disjoint manifolds. Formally, let a redundant inverse kinematic solution be denoted as the union of disjoint r-dimensional manifolds:

$$f^{-1}(\mathbf{x}) = \bigcup_{i}^{n_{sm}} M_i(\overline{\psi}); \tag{7}$$

where $M_i(\overline{\psi})$ is the i^{th} r-dimensional manifold in the inverse kinematic preimage, and $M_i \cap M_j = \emptyset$ when $i \neq j$. Each of the preimage manifolds physically corresponds to a "self-motion," which is a continuous motion of the manipulator joints which leaves the end-effector motionless.

> **Definition:** Each of the disjoint r-dimensional manifolds in the inverse kinematic preimage will be termed a *self-motion manifold.*

n_{sm} is the number of self-motions in the preimage (bounds on the value of n_{sm} will be considered in Section 4). Each

[1] For a non-redundant manipulator, a *regular point of* f is a configuration, $\overline{\theta}$, for which $f(\overline{\theta})$ is not singular (the Jacobian of f is full rank). A *regular value* is an end-effector location $\mathbf{x} = f(\overline{\theta})$ where $\overline{\theta}$ is a regular point. A *critical point* is a configuration, $\overline{\theta}$, such that $f(\overline{\theta})$ is singular. A *critical value* is an end-effector location $\mathbf{x} = f(\overline{\theta})$ where $\overline{\theta}$ is a critical point. For redundant manipulators, these definitions are extended so that a regular value has all regular points in its preimage, a critical value has all critical points in its preimage, and a *coregular* value is an $\mathbf{x}$ which has both regular and critical points in its preimage.

M_i can be parametrized by a set of r independent parameters, $\overline{\psi} = \{\psi_1, \cdots, \psi_r\}$, which can be thought of as a natural coordinate system for the self-motions. For given x, the parametrization is generally unique (up to isomorphism), but the parametrization can vary as x varies in the workspace.

The self-motion manifolds are best illustrated using two examples: a planar 3R manipulator (Figure 4) which is redundant with respect to the position of its end-effector, and a 4R regional manipulator which is similar to an "elbow" manipulator (Figure 5). The self-motion manifolds of the planar manipulator can be computed as follows. Let ψ, which is the orientation of the third link relative to a fixed reference system, be the parameter describing the internal motion of the manipulator. There are two possible sets of joint angles, $\overline{\theta}_a = \{\theta_{1a}, \theta_{2a}, \theta_{3a}\}$ and $\overline{\theta}_b = \{\theta_{1b}, \theta_{2b}, \theta_{3b}\}$, which place the end-effector at (x_{ee}, y_{ee}) with given ψ. These solutions can be determined by evaluating the following equations:

$$
\begin{aligned}
R_2 &= \sqrt{x_{ee}^2 + y_{ee}^2 + l_3^2 - 2l_3(x_{ee}\cos\psi + y_{ee}\sin\psi)} \\
\alpha &= atan2(y_{ee} - l_3\sin\psi, x_{ee} - l_3\cos\psi) \\
\gamma &= \cos^{-1}\left(\frac{l_1^2 + l_2^2 - R_2^2}{2l_1 l_2}\right) \qquad \eta = \cos^{-1}\left(\frac{l_1^2 + R_2^2 - l_2^2}{2l_1 R_2}\right) \\
\overline{\theta}_a &= \{(\alpha+\eta), (\gamma-\pi), (\psi-\alpha-\eta-\gamma+\pi)\} \\
\overline{\theta}_b &= \{(\alpha-\eta), (\pi-\gamma), (\psi-\alpha+\eta+\gamma-\pi)\}
\end{aligned}
\tag{8}
$$

where l_1, l_2, l_3 are the lengths of links 1, 2, and 3. As ψ is swept through its feasible range of $[-\pi, \pi]$, equations (8) will generate two 1-dimensional manifolds in $\mathcal{C}$. These manifolds may remain separate for all values of ψ, in which case there are two disjoint self-motions, or the two branches may meet at two points (corresponding to the singularities of the non-redundant $2R$ planar manipulator subchain formed by links 1 and 2), to form one self-motion manifold.

Figure 4 shows the self-motion manifolds of this planar manipulator (embedded in the configuration space 3-torus) for two different locations of the end-effector. The inverse image of point 1 contains two distinct self-motion manifolds (which appear as non-closed curves because of the cubic 3-torus representation), while the inverse image of point 2 contains only one self-motion. The two distinct self-motion manifolds in the preimage of point 1 physically corresponds to "up elbow" and "down elbow" self-motions which are an analogous generalization of the "up elbow" and "down elbow" configurations of a non-redundant two-link manipulator. Self-motions can be thought of as a natural generalization of the non-redundant manipulator concept of "pose" to redundant manipulators. In both cases, the self-motion manifolds are diffeomorphic[2] to a circle. However, the preimage of point 1 contains a 2π joint rotation while the other preimage does not.

Now consider the $4R$ manipulator in Figure 5. The kinematic parameters of this arm (following the conventions in [9]) are: $\alpha_0 = 0$; $\alpha_1 = \alpha_2 = \pi/2$; $\alpha_3 = -\pi/2$; $a_0 = a_1 = a_2 = 0$; $a_3 = a_4 = l$; $d_1 = d_2 = d_3 = d_4 = 0$. Let the self-motion parameter, ψ, be the angle between the plane containing the third and fourth links and the vertical plane passing through joint axis 1. The following equations compute four inverse kinematic solutions, $\{\theta_{1a}, \theta_{2a}, \theta_{3a}, \theta_{4a}\}, \{\theta_{1b}, \theta_{2b}, \theta_{3b}, \theta_{4a}\}, \{\theta_{1c}, \theta_{2c}, \theta_{3c}, \theta_{4b}\}, \{\theta_{1d}, \theta_{2d}, \theta_{3d}, \theta_{4d}\}$, given $\mathbf{x} = (x_{ee}, y_{ee}, z_{ee})$ and a value for the self-motion parameter, ψ.

[2] A smooth map $f: X \to Y$ (where X and Y are manifolds) is a diffeomorphism if it is one-to-one and onto, and $f^{-1}: Y \to X$ is smooth. X and Y are diffeomorphic if such an f exists.

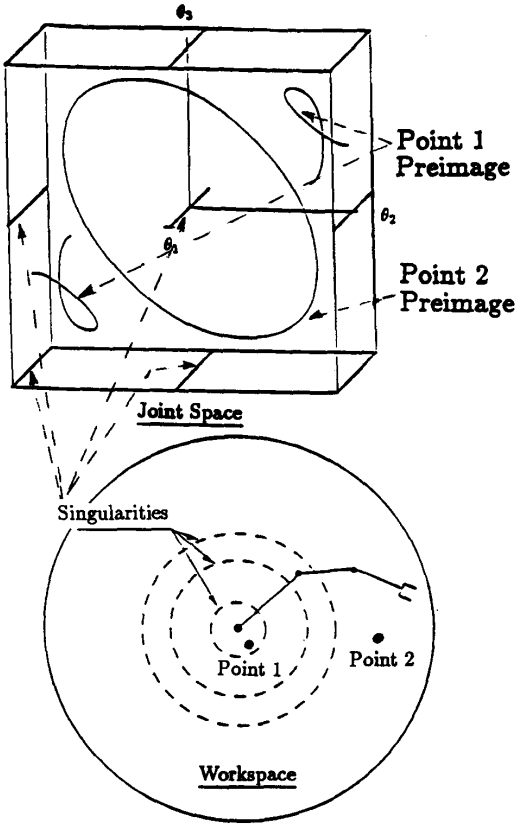

Figure 4: Self-Motions of Planar $3R$ Manipulator

Define the following variables, which are purely functions of the end-effector location and the link length parameter, l.

$$
\begin{aligned}
R_2 &= \sqrt{x_{ee}^2 + y_{ee}^2} & R_3 &= \sqrt{x_{ee}^2 + y_{ee}^2 + z_{ee}^2} \\
\cos\beta &= x_{ee}/R_2 & \sin\beta &= y_{ee}/R_2 \\
\cos\xi &= R_2/R_3 & \sin\xi &= z_{ee}/R_3 \\
\cos\gamma &= R_3/2l & \sin\gamma &= (1/2l)\sqrt{4l^2 - R_3^2}
\end{aligned}
\tag{9}
$$

There are two unique values of θ_4 which satisfy the inverse kinematic function:

$$\theta_{4a} = 2\ atan2(\sin\gamma, \cos\gamma); \qquad \theta_{4b} = -\theta_{4a} \tag{10}$$

There are four unique values of θ_2 (two corresponding to each value of θ_4 in (10)):

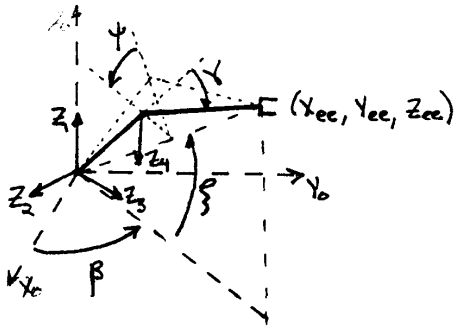

Figure 5: Geometry of a $4R$ Elbow-Like Manipulator

$$\begin{aligned} \theta_{2a} &= \cos^{-1}[\sin\xi\sin\gamma - \cos\xi\cos\gamma\cos\psi] \\ \theta_{2c} &= \cos^{-1}[\sin\xi\sin\gamma + \cos\xi\cos\gamma\cos\psi] \qquad (11) \\ \theta_{2b} &= -\theta_{2a} \qquad \theta_{2d} = -\theta_{2c}. \end{aligned}$$

There are four corresponding values of θ_1 which can be computed as follows:

$$\begin{aligned} \theta_{1a} &= \text{atan2}\left[\frac{-\sin\psi\cos\gamma}{\sin\theta_{2a}}, \frac{-(\cos\xi\sin\gamma + \sin\xi\cos\gamma\cos\psi)}{\sin\theta_{2a}}\right] \\ \theta_{1c} &= \text{atan2}\left[\frac{\sin\psi\cos\gamma}{\sin\theta_{2c}}, \frac{(-\cos\xi\sin\gamma + \sin\xi\cos\gamma\cos\psi)}{\sin\theta_{2c}}\right] \\ \theta_{1b} &= \theta_{1a} \pm \pi \qquad \theta_{1d} = \theta_{1c} \pm \pi \end{aligned} \qquad (12)$$

Similarly, there are four corresponding values of θ_3 which can be computed as follows:

$$\begin{aligned} \theta_{3a} &= \text{atan2}\left[\frac{-\cos\xi\sin\psi}{\sin\theta_{2a}}, \frac{\sin\xi\cos\gamma + \cos\xi\sin\gamma\cos\psi}{\sin\theta_{2a}}\right] \\ \theta_{3c} &= \text{atan2}\left[\frac{\cos\xi\sin\psi}{\sin\theta_{2c}}, \frac{\sin\xi\cos\gamma + \cos\xi\sin\gamma\cos\psi}{\sin\theta_{2c}}\right] \\ \theta_{3b} &= \theta_{3a} \pm \pi \qquad \theta_{3d} = \theta_{3c} \pm \pi. \end{aligned} \qquad (13)$$

The inverse solution is real for all values of ψ in the range $[-\pi, \pi]$. The four distinct self-motions of this manipulator can be generated by continuously sweeping ψ through its 2π range for fixed (x_{ee}, y_{ee}, z_{ee}). Figure 6 shows the cubic representation of the projection of these four self-motions onto the θ_1-θ_2-θ_3 and θ_2-θ_3-θ_4 3-tori (for the case in which $l = 1.0$, $(x_{ee}, y_{ee}, z_{ee}) = (0.0, 1.0, 0.9)$).

4. Determining the Number of Self-Motions

What physical conditions determine whether there are one or two self-motion manifolds in Figure 4, and what is an upper bound on the number of self-motions? The inverse kinematic solution in (8) was found by a reassembly approach. That is, the the end-effector is fixed to (x_{ee}, y_{ee}) by a virtual revolute joint and the structure is broken into two subcomponents (at joint 3), a non-redundant $2R$ manipulator and a $1R$ link. Let C_3 denote the circle of joint 3 locations formed by rotating link 3 about (x_{ee}, y_{ee}). If C_3 lies entirely within the workspace of the $2R$ subchain (Figure 7(a)), the $2R$ subchain can position joint 3 on C_3 (to insure consistent reassembly of

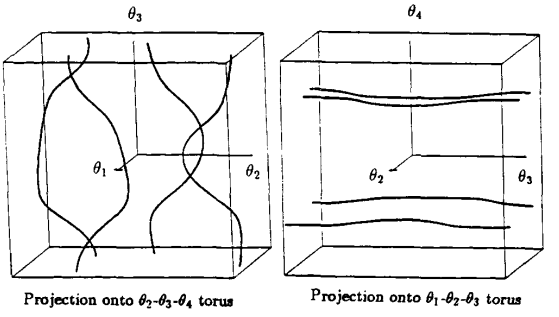

Figure 6: $4R$ Manipulator Self-Motion Manifolds

the manipulator) in two distinct ways, and consequently the inverse image of (x_{ee}, y_{ee}) consists of two disjoint self-motion manifolds, each containing a complete 2π rotation of joint 2. In Figure 7(b) only one continuous arc segment of C_3 is within the workspace of the $2R$ subchain. The $2R$ subchain can reach points on this arc in two configurations. However, the $2R$ subchain is in a singular configuration at the two points where C_3 intersects the $2R$ workspace boundary. Both inverse preimages of the arc join at the subchain singularities (since $\theta_2 = 0$ in both cases) to form one self-motion manifold. In Figure 7(c) C_3 intersects the workspace of the $2R$ subchain in two disjoint arcs. Because the $2R$ subchain is singular when the arcs intersect the $2R$ workspace boundaries, there is only one solution on each arc, resulting in a total of two solutions. [Note, the manipulators in Figure 7 are not all drawn to scale.]

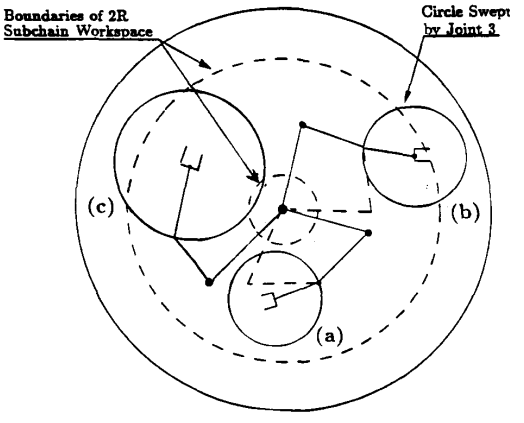

Figure 7: Determining the Number of Self-Motions

The preimage manifolds of an nR planar manipulator ($n \geq 4$) can be analyzed by induction. Divide a $4R$ manipulator at the origin of link frame 4 into a $3R$ redundant subchain (links 1, 2, and 3) and a single link (link 4). Let C_4 be the circle formed by rotating link 4 about (x_{ee}, y_{ee}). The $3R$ subchain can position joint 4 at each point of C_4 with as many as two distinct self-motions, yielding as many as two 2-dimensional preimages. These preimages may coalesce at a subchain singularity to form a single connected preimage, or the $3R$ subchain may only have one self-motion on C_4. By

induction, this analysis can be extended to planar manipulators with 5 or more joints to show that there are at most two self-motion manifolds for all redundant planar manipulators. Furthermore, this physical reasoning can be extended to spherical, regional, and spatial manipulators [2] to show that:

Theorem 1: *For any regular* $\mathbf{x} \in \mathcal{W}$, *ann-revolute-jointed redundant manipulator can have no more self-motions than the maximum number of inverse kinematic solutions of a non-redundant manipulator of the same class. That is, redundant planar, spherical, regional, and spatial manipulators can respectively have as many as 2, 4, and 16 distinct self-motions.*

As n increases, the number of self motion generally decreases. In the limit as $n \rightarrow \infty$, a manipulator is akin to a string, which has only one self-motion.

5. The Geometry of a Self-motion

The self-motion manifolds in Figures 4 and 6 were diffeomorphic to circles. What shape do the self-motion manifolds have in general? Let $f_m^{-1}(\mathbf{x})$ be the inverse kinematic function of an m-revolute-jointed non-redundant manipulator of a given class (e.g., spherical, regional, or spatial). Lock the last r joints of a redundant manipulator at joint angles $(\theta_{(m+1)_o}, \cdots, \theta_{n_o})$, and solve the non-redundant inverse kinematic problem for the first m joints:

$$f_m^{-1}(\mathbf{x} - g(\theta_{(m+1)_o}, \cdots, \theta_{n_o})) \;=\; f_m^{-1}(\mathbf{x}_{eff}) \qquad (14)$$

where g is a function which computes the length of the subchain formed by the last r joints. In other words, the m-link non-redundant sub-chain must place the m^{th} link frame at effective location $\mathbf{x}_{eff}$ to consistently reassemble the entire n-link manipulator whose last r-links are locked. The self-motion manifolds can be generated by sweeping the last r joints through their 2π ranges (Let C_r be the surface generated by g as the last r joints rotate). Because f_m^{-1} is a local diffeomorphism [2], the self-motions manifolds must be locally diffeomorphic to the joint space manifold of $\theta_{m+1}, \cdots, \theta_n$, which is an r-torus. The exact global geometry depends on several factors.

If C_r does not intersect a critical value of f_m, by an inductive argument it can be shown that the self-motion manifolds are globally diffeomorphic to an r-torus. If $r = 1$ and C_r does not intersect a critical value of the m-joint subchain, the self-motion manifold must be a closed compact 1-dimensional manifold in the configuration space, which is necessarily diffeomorphic to a circle. Now consider $r = 2$. If C_r doesn't intersect a critical value of the m-joint subchain, the subchain formed by the first $m + 1$ joints will have self-motions which are diffeomorphic to a circle (since the $m+1$ subchain can reach every point on the surface formed by rotating the last joint with no singularities). The self-motion for $r = 2$ is the product of the $m + 1$ chain self-motions and the self-motion of the last link (which necessarily rotates by 2π in $\mathcal{C}$), and must be a 2-torus. This argument can be extended by induction.

The situation becomes more complicated when C_r intersects a critical value of f_m, which is typically the case. If C_r intersects a critical value which is not a workspace boundary critical value (so that C_r lies entirely in $\mathcal{W}$), two solutions of f_m meet at the critical value, which in effect glues the preimages of two arcs of C_r together. In this case the self-motion manifold typically is still a torus. However, when C_r intersects a workspace boundary critical value of f_m, the self-motions are a product of the self-motion of a subchain self-motion and an arc (since the last joint(s) can not completely rotate if C_r does not lie entirely in $\mathcal{W}$). For $r = 2$, the self-motion assumes a spherical shape near the workspace boundary. For $r > 2$, the self-motion geometry can become quite complex.

Remark: *Revolute-jointed manipulator self-motion manifolds are typically diffeomorphic to an r-torus,* T^r. *However, near workspace boundaries, the self-motion manifolds may assume spherical or even more complicated shapes.*

6. Geometric Interpretation of the Null Space

Many instantaneous redundancy resolution techniques employ the null space of the manipulator Jacobian. The null space has a simple interpretation as the self-motion manifold tangent space. The joint coordinates of the self-motion manifold can be expressed as functions of the self-motion parameters:

$$M_i(\overline{\psi}) = [\, \theta_1(\overline{\psi}) \quad \cdots \quad \theta_n(\overline{\psi}) \,]^T = \overline{\theta}(\overline{\psi}). \qquad (15)$$

The tangent space to M_i at some $\overline{\theta}_o = \overline{\theta}(\overline{\psi}_o)$ is:

$$\frac{dM_i(\overline{\psi}_o)}{d\overline{\psi}} d\overline{\psi} \;=\; \frac{d\overline{\theta}(\overline{\psi}_o)}{d\overline{\psi}} d\overline{\psi} \qquad (16)$$

where $d\overline{\psi} \in \mathbf{R}^r$. If f is restricted to the self-motion manifold, then:

$$d\mathbf{x}(\overline{\psi}_o) \;=\; \frac{df(\overline{\theta}(\overline{\psi}_o))}{d\overline{\theta}} \frac{d\overline{\theta}(\overline{\psi}_o)}{d\overline{\psi}} d\overline{\psi} \;=\; \mathbf{J}(\overline{\theta}_o) \frac{d\overline{\theta}(\overline{\psi}_o)}{d\overline{\psi}} d\overline{\psi} \qquad (17)$$

However, when f is restricted to a self-motion manifold, $d\mathbf{x}(\overline{\psi}_o)$ must be zero, and therefore $(d\overline{\theta}(\overline{\psi}_o)/d\overline{\psi}) d\overline{\psi}$, which is the tangent space of $M_i(\overline{\psi})$, must be in the null space of the Jacobian.

Remark: The null space of the Jacobian matrix, evaluated at a particular joint configuration, $\overline{\theta}_o$, is the tangent to the self-motion manifold at $\overline{\theta}_o$. The collective null spaces of one self-motion is the *tangent bundle*[3] of the self-motion manifold. The set of all Jacobian null spaces over a fixed end-effector location will be the union of all self-motion tangent bundles.

For example, the null space of the manipulator in Figure 4 at $\overline{\theta}_o$ is a line, $\mathbb{R}^1$, tangent to the self-motion manifold at $\overline{\theta}_o$. The collection of all null spaces for one self-motion of this manipulator is diffeomorphic to $S^1 \times \mathbb{R}^1$, a cylinder. Figure 8 shows the tangent spaces of the self-motion manifold over point 2 in Figure 4.

[3] For an n-dimensional manifold X, the tangent bundle of X, denoted $T(X)$, is the subset of $X \times \mathbf{R}^n$ defined by $T(X) = \{(x, v) \in X \times \mathbf{R}^n : v \in T_x(x)\}$. In other words, the tangent bundle of X is an $2n$-dimensional manifold formed by "tacking on" to every $x \epsilon X$ a copy of the tangent space at x.

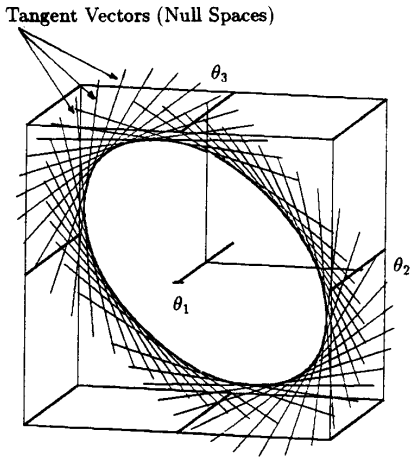

Figure 8: $3R$ Manipulator Null Spaces

7. Self-motion Homotopy Classes

In the example of Figure 4, the self-motion manifolds over point 1 included a 2π joint rotation, while the self-motions over point 2 did not. Both self-motions are diffeomorphic to a circle, but they are not homotopic.[4] The self-motions of point 1, which wrap around a generator of $\mathcal{C}$, can not be continuously deformed on the surface of the configuration space torus to the self-motions of point 2. Self-motions which are homotopic to each other form a *homotopy class.* The notion of a homotopy class has previously been used in [10] to characterize different redundancy resolution paths. When $r = 1$, the homotopy classes of the self-motion manifolds can be interpreted as elements in the fundamental group[5] of $\mathcal{C}$. The fundamental group of an n-torus is $\mathbf{Z} \times \mathbf{Z} \times \cdots \times \mathbf{Z}$ [11]. Therefore, the homotopy class of a self-motion can be specified by an n-tuple of integers $(I_1, I_2, \cdots, I_n)$, where I_j represents how many integral times the self-motion manifold wraps around the j^{th} configuration space generator. While a definite upper bound on the number of homotopy classes has not yet been determined, it appears that there are at most $2^{(n-2)}$ different self-motion homotopy classes for a given manipulator [6]. When the relative degree of redundancy is greater than 1, there does not appear to be a simple way to characterize the homotopy classes of self-motions.

8. Coregular Self-Motions and $\mathcal{C}$-Bundles

For redundant manipulators, when $\mathbf{x}$ is a critical value, the kinematic preimage may contain both critical and regular points (thereby enabling singularity avoidance). Such $\mathbf{x}$ are termed *coregular*, and the self-motions in the preimage of such points are termed *coregular self-motions.* However, a coregular preimage does not properly form a manifold. The structure of coregular self-motions can be investigated by considering the $3R$ planar manipulator self-motions as the end-effector nears a singularity (which is not a workspace boundary singularity). At the singularity, two self-motions (which are diffeomorphic to circles) join at a point, to form a "bouquet of circles," or a curve which is diffeomorphic to a figure 8. Only the waist of the figure 8 is a critical point, whereas the other points in the figure 8 are coregular.

The preimage of an entire critical value manifold (which is formed by sweeping $f^{-1}(\mathbf{x})$ along the critical value manifold) is a continuous surface, termed a *coregular surface.* Coregular surfaces are not manifolds, but by virtue of their dimension, they can separate the configuration into disjoint regions. Figure 9 illustrates all of the coregular surfaces for

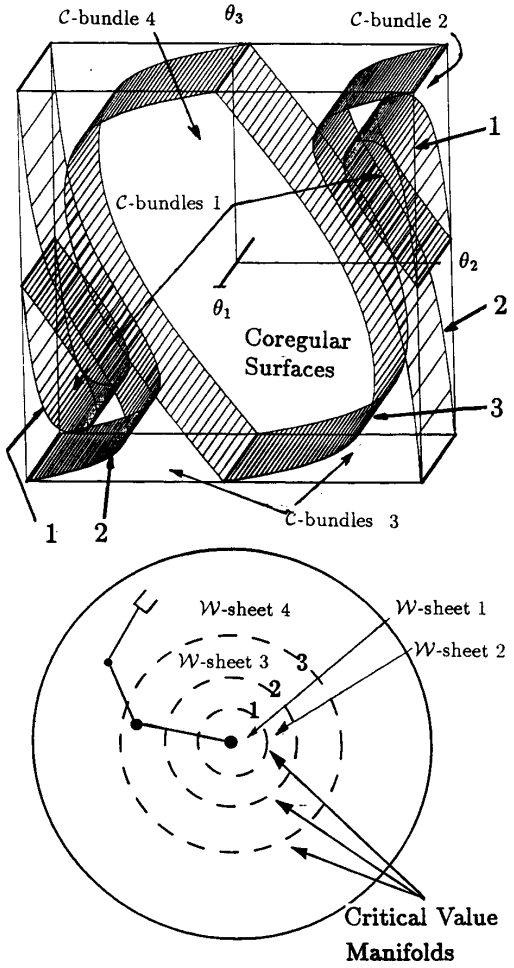

Figure 9: Coregular Surfaces, $\mathcal{C}$-bundles, and $\mathcal{W}$-sheets of a $3R$ Manipulator

[4] Two maps, $f_0: X \to Y$ and $f_1: X \to Y$ are homotopic if there exists a smooth map, $F: X \times I \to Y$ such that $F(x,0) = f_o(x)$ and $F(x,1) = f_1(x)$. In other words, f_0 can be deformed to f_1 through a smoothly evolving family of maps.

[5] For path connected manifolds, such as $\mathcal{C}$, let Ω, denote the set of all closed loops in $\mathcal{C}$. All homotopic loops in $\mathcal{C}$ form a *path component* in the loop space, which is an equivalence class of loops under homotopy. The fundamental group of $\mathcal{C}$ is the group of loop equivalence classes: $\pi_1(\mathcal{C}) = \Omega/\sim$ (loop homotopies) [11].

the $3R$ manipulator of Figure 4. In [2] it is shown that the coregular surfaces divide the configuration space into disjoint regions which are fibre bundles. [6] In this context, a fibre bundle is a collection of homotopic self-motion manifolds. Further, these fibre bundles are preimages of workspace subregions bounded by critical values.

> **Definition:** A region in $\mathcal{C}$ bounded by a coregular surface is termed a $\mathcal{C}$-bundle. A region in $\mathcal{W}$ bounded by critical value manifolds is termed a $\mathcal{W}$-sheet, and the preimage of a $\mathcal{W}$-sheet consists of one or more $\mathcal{C}$-bundles [2].

The number of $\mathcal{C}$-bundles over a $\mathcal{W}$-sheet is equivalent to the number of distinct self motions. In Figure 9, $\mathcal{W}$-sheets 1 and 3 have two $\mathcal{C}$-bundles in their preimages ($\mathcal{C}$-bundles 1 and 3), indicating the presence of two self-motions in these regions. $\mathcal{W}$-sheets 2 and 4 have only one $\mathcal{C}$-bundle preimage. Thus, the number of distinct self-motions is constant in a $\mathcal{W}$-sheet and only varies when crossing a critical value surface into another $\mathcal{W}$-sheet. These concept generalize to spherical, regional, and spatial manipulators as well.

9. Discussion

This global kinematic investigation is primarily aimed at developing new insight into redundant manipulator kinematics and redundancy resolution problems and techniques. Space limitations prevent an extensive discussion, but some simple applications of these ideas are outlined. Consider instantaneous redundancy resolution methods based on (4) for redundancy resolution with fixed $\mathbf{x}$ and objective function $g(\overline{\theta})$ (which might be a measure of mechanical advantage for example). The goal is to find the arm configuration which optimizes $g(\overline{\theta})$ for given $\mathbf{x}$. If the manipulator starts in some configuration, $\overline{\theta}_o$, which is not optimal, then a small increment in $\overline{\theta}$ which moves the arm toward the optimal configuration can be computed as:

$$\delta\overline{\theta} = \alpha(\mathbf{I} - \mathbf{J}^{\dagger}(\overline{\theta}_o)\mathbf{J}(\overline{\theta}_o))\nabla g(\overline{\theta}_o) \qquad (18)$$

where α is a scalar. Thus, redundancy resolution based on (4) can be interpreted as a first order gradient search on the self-motion manifold. First order gradient searches are prone to finding local, and not global optimum. Further, the instantaneous techniques can only search over one self-motion manifold, whereas the true optimum of $g(\overline{\theta})$ might lie on another self-motion manifold, and therefore be missed by the instantaneous approach.

The ideas in Sections 6 and 7 are quite useful for predicting the variation of kinematic properties, such as the number and physical nature of self-motions, throughout $\mathcal{W}$. All self-motions in a $\mathcal{C}$-bundle are homotopic, implying that the physical motion of the links in a self-motion are similar when the end-effector remains within one $\mathcal{W}$-sheet. However, when crossing co-regular surfaces in $\mathcal{C}$ (or critical value manifolds in $\mathcal{W}$), the homotopy class of the self-motion can change, and consequently, the physical motion of the links can change as well. This phenomenon can be demonstrated by considering a $7R$ arm which is formed by adding a $3R$ wrist (with finite hand length) to the $4R$ manipulator of Figure 5. In most parts of the workspace, the self-motion consists of a rotation of the plane containing links 3 and 4 about the line between the shoulder and the wrist. However, when axis 7 aligns with link 4, axes 1, 2, 3, and 4 are locked, and the self-motion manifests itself as a self-motion of the wrist joints. This self-motion is physically very different from the nominal self-motion, and is separated in $\mathcal{C}$ from the nominal self-motions by a coregular surface. By analyzing the singularities (a method is given in [2] for synthesizing the singularities of arbitrary nR), it is possible to predict where the physical nature of the self-motion may drastically change. This might be important information for path planning operations which utilize redundancy, and the method outlined in this paper are useful for investigating these kinds of global behaviors for manipulators with geometries more complicated than the simple $7R$ model described above.

[6] A *fibre bundle* is a four-tuple, $\xi = (\tilde{X}, X, F, p)$, consisting of a *total space* $\tilde{X}$, a *base space* X, a *fibre* F, and a *bundle projection* $p: \tilde{X} \rightarrow X$ such that there exists an open covering $\{U\}$ of X, and for each $U \in \{U\}$, a homeomorphism $\phi: U \times F \rightarrow p^{-1}(U)$ such that the composition of maps, $U \times F \rightarrow^{\phi} p^{-1}(U) \rightarrow^{p} U$, is a projection to the first factor, U.

Acknowledgements

The author gratefully acknowledges many useful contributions and suggestions by Prof. Bernard Roth, Dr. Madhu Raghavan, Dr. Charles Wampler, Dr. Ken Kreutz, and the anonymous reviewers of earlier drafts. Much of this work was supported by the System Development Foundation, and an IBM faculty development grant.

10. References

[1] C.A. Klein and C.H. Huang, "Review of the Pseudoinverse for Control of Kinematically Redundant Manipulators," *IEEE Transactions on Systems, Man and Cybernetics*, March, 1983.

[2] J. W. Burdick, Kinematic Analysis and Design of Redundant Robot Manipulators, Ph.D. Thesis, Department of Mechanical Engineering, Stanford University, March 1988.

[3] D. H. Gottlieb, "Robots and Topology," *Proceedings of the IEEE International Conference on Robotics and Automation*, April 7-10, 1987, San Francisco, CA, vol. 3, pp. 1689-1691.

[4] D. R. Baker and C.W. Wampler, "Some Facts Concerning Inverse Kinematics for Redundant Manipulators," *Proceedings of the IEEE International Conference on Robotics and Automation*, March 30-April 3, 1987, Raleigh, NC.

[5] C. Wampler, "On the Inverse Kinematics of Redundant Manipulators," to appear in the proceedings of the *Nato Workshop on Redundancy in Robotics: Sensing, Design, and Control*, Salo, Italy, June 26, July 1, 1988, Springer Verlag.

[6] J. W. Burdick, "On the Kinematics of Redundant Manipulators: a Global Mapping Approach," in preparation.

[7] E.J.F. Primrose, "On the Input-Output Equations of the General 7R-Mechanism, *Mechanism and Machine Theory*, vol. 21, no. 6, pp. 509-510, 1986.

[8] Victor Guillemin and Alan Pollack, Differential Topology, Prentice-Hall, Inc., Englewood Cliffs, New Jersey, 1974.

[9] J. J. Craig, Introduction to Robotics: Manipulation and Control, Addison-Wesley, Reading, Mass., 1986.

[10] J. Baillieul and D. P. Martin, "Issues in the Control of Kinematically Redundant Mechanisms," proceedings of the *Nato Workshop on Redundancy in Robotics: Sensing, Design, and Control*, Salo, Italy, June 26, July 1, 1988, Springer Verlag.

[11] W.S. Massey, Algebraic Topology: An Introduction, Springer-Verlag, New York, 1967.